A&A, 707, A62 (2026)
https://doi.org/10.1051/0004-6361/202557266
© The Authors 2026

Astronomy & Astrophysics

eROSITA selection of new period-bounce cataclysmic variables

First follow-up confirmation using TESS and SDSS

Daniela Muñoz-Giraldo[1,⋆], Beate Stelzer[1], Axel Schwope[2], Santiago Hernández-Díaz[1], Scott F. Anderson[3], and Sebastian Demasi[3]

[1] Institut für Astronomie und Astrophysik, Eberhard Karls Universität Tübingen, Sand 1, 72076 Tübingen, Germany
[2] Leibniz-Institut für Astrophysik Potsdam (AIP), An der Sternwarte 16, 14482 Potsdam, Germany
[3] Department of Astronomy, University of Washington, Box 351580, Seattle, WA 98195, USA

Received 16 September 2025 / Accepted 21 January 2026

ABSTRACT

Context. Between 40% and 80% of cataclysmic variables (CVs) are expected to have evolved past the period-minimum and contain a degenerate donor. However, observational surveys for CVs have only been able to detect a few of these highly evolved "period-bouncers", most likely due to the intrinsic faintness associated with their predicted low mass accretion rates.
Aims. We searched for new period-bouncers in optical white dwarf (WD) catalogs. Our findings will establish if the missing population of this underrepresented type of CVs can be identified through these existing catalogs.
Methods. We have produced an initial selection of high-likelihood period-bounce candidates based on our multiwavelength period-bouncer scorecard and selection cuts including X-ray data from the extended ROentgen Survey with an Imaging Telescope Array (eROSITA) on board the Spektrum-Roentgen-Gamma spacecraft (SRG). We have laid out a clear path based on three main requirements (classification as a CV, determination of an orbital period, and detection of a very late-type donor) that should result in the confirmation of several of these candidates, and that will serve as a reference for future searches of period-bouncers.
Results. Our selection method of identifying new period-bouncers in WD catalogs successfully retrieves already known period-bouncers found in the *Gaia* DR3 WD catalog, and also identifies five new period-bouncers classified in the literature only as CVs, and 137 high-likelihood period-bounce candidates that were classified in the literature only as single WDs. Our path for confirming these candidates has already produced its first successful result with the confirmation of GALEX J125751.4-283015 as a new period-bouncer. Several other candidates have already fulfilled at least one of our three requirements, making their future confirmation likely.
Conclusions. Our search for period-bouncers using the X-ray eROSITA emission of objects in optical WD catalogs has led to the confirmation of six new period-bouncers identified from the *Gaia* DR3 WD catalog (five previously known CVs and one WD candidate), an 18% increase that brings the present population to 39 systems. Both the selection method for period-bounce candidates and the confirmation path that we outlined will aid in future searches for new period-bounce candidates, contributing to the goal of resolving the discrepancy between the high predicted number of period-bouncers and the low number of these systems successfully observed to date.

Key words. stars: late-type – novae, cataclysmic variables – white dwarfs

1. Introduction

Cataclysmic variables (CVs) are close binary systems in which a white dwarf (WD) accretes material from a late-type companion star that fills its Roche lobe (Warner 1995). As was described by Paczynski (1976), CVs form as a result of a common envelope (CE) phase during the binary's evolution. In this phase, the envelope of a more massive, Roche-lobe filling primary star expands and engulfs its companion. After the ejection of the envelope, a post-CE binary is left consisting of the evolved core of the primary star (now a WD) and a low-mass, main-sequence companion. The friction generated during the CE phase causes a loss of angular momentum and energy, which drives a significant decrease in the orbital separation of the binary, such that, once it becomes small enough to permit mass transfer from the companion to the WD, the system morphs into a CV.

The subsequent evolution of CVs is driven by angular momentum losses toward increasingly short separations (and thus orbital periods, $P_{\rm orb}$), resulting in a evolution track from longer orbital periods to shorter ones (Paczynski 1976, Kolb 1993, Warner 1995, Knigge et al. 2011). Starting as a CV with long orbital periods ($P_{\rm orb} > 3$ h), the system will evolve until it reaches the period gap ($2\,{\rm h} < P_{\rm orb} < 3\,{\rm h}$), becoming a detached binary. The system reemerges at the lower end of the period gap as an active CV when the donor is once again filling its Roche lobe (Kolb et al. 1998). The evolution continues toward even shorter periods through angular momentum loss due to gravitational radiation, until the system reaches a period minimum located at $P_{\rm min} \approx 80$ min (see e.g., Howell et al. 2001; Patterson 2011; Pretorius et al. 2013; Goliasch & Nelson 2015; McAllister et al. 2019; Pala et al. 2020, 2022). At this point, the donor is out of thermal equilibrium due to its mass-loss timescale becoming much shorter than its thermal timescale, causing the donor to stop shrinking in response to mass loss (King 1988). The very late-type donor, unable to sustain hydrogen burning, becomes a brown dwarf (Howell et al. 2001), with this change in internal structure resulting in the increase in the system's orbital separation and consequently in the CV bouncing back

⋆ Corresponding author:
munoz-giraldo@astro.uni-tuebingen.de

Open Access article, published by EDP Sciences, under the terms of the Creative Commons Attribution License (https://creativecommons.org/licenses/by/4.0), which permits unrestricted use, distribution, and reproduction in any medium, provided the original work is properly cited.
This article is published in open access under the Subscribe to Open model. Subscribe to A&A to support open access publication.

to longer orbital periods. The systems that go through this process of "bounce-back" to longer periods are known as period-bouncers (Patterson 1998).

The majority of the CV population, according to theoretical models describing CV evolution, is expected to be made up of period-bouncers. However, the actual contribution from period-bouncers to the total CV population is highly disputed, with estimations ranging between 40% and 80%, depending heavily on assumptions about the formation, evolution, and system parameters (see e.g., Kolb 1993; Goliasch & Nelson 2015; Belloni et al. 2020). To this date, there are 33 confirmed period-bouncers, including 21 bona fide period-bouncers for which a reliable detection of a late-type donor strengthens their classification (see Table 1). Estimates place the percentage of observed period-bouncers between 3% and 25% (Inight et al. 2023b, Pala et al. 2020, Rodriguez et al. 2025), establishing these objects as a minority subtype of CVs.

The late-type donors (late M to T dwarfs) of period-bouncers are characterized for presenting emission in bands such as X-ray (Audard et al. 2007, De Luca et al. 2020) and optical (Girven et al. 2011, Inight et al. 2023a, Inight et al. 2023b) that is hardly detectable with present-day instrumentation, where the emission is dominated by the accretion structures and WD in each case, respectively. Therefore, the detection of X-ray emission arising from an optically identified WD is a key diagnostic of ongoing mass accretion in a WD-dominated binary system, and hence it is the most promising path for the identification of period-bouncers.

Optical surveys such as *Gaia* or the Sloan Digital Sky Survey (SDSS) have produced vast catalogs of WDs (see e.g., Kepler et al. 2015; Jiménez-Esteban et al. 2018; Gentile Fusillo et al. 2019, 2021; Kepler et al. 2021). These catalogs can be used as a starting point in the search for the missing population of period-bouncers, as is demonstrated in Inight et al. (2023b). Particularly, we are searching for emission detected by an all-sky X-ray survey that can prove the systems in these catalogs are not single cool WDs but potential interacting binaries. The launch of the extended ROentgen Survey with an Imaging Telescope Array (eROSITA; Predehl et al. 2021) on board the Spektrum-Roentgen-Gamma mission (SRG; Sunyaev et al. 2021) has allowed us access to large statistical samples of X-ray sources. The eROSITA detections of confirmed period-bouncers (Muñoz-Giraldo et al. 2023, Muñoz-Giraldo et al. 2024a, Muñoz-Giraldo et al. 2024b) proved the capabilities of this instrument in the identification and confirmation of such faint sources, leading to an 82% increase in the population of eROSITA-detected period-bouncers.

The main focus of this study is to find the population of period-bouncers that is potentially hiding in WD catalogs. To this end, we have used the selection cuts and period-bouncer scorecard by Muñoz-Giraldo et al. (2024a) to identify high-likelihood period-bounce candidates, as well as other interesting X-ray sources such as single WDs, wide WD-main sequence binaries, WD-WD binaries, ultracompact binaries, among others. In our effort to confirm the period-bounce candidates, we have established three main requirements that a candidate needs to fulfill in order to be successfully reclassified from a single WD into a period-bouncer. Observational follow-up campaigns are already on their way to ensure we have the data necessary to determine if our candidates fulfill these requirements. As more candidates are confirmed as period-bouncers, it will also provide a reliable observational dataset that could be used for any future theoretical modeling of the late-phase of CV evolution.

Our selection of period-bounce candidates is introduced in more detail in Sect. 2, providing specific information on the WD catalog and scorecard used for this purpose. In Sect. 3 we discuss the eROSITA X-ray detections of the selected candidates that lead to the identification of high-likelihood period-bounce candidates. A breakdown of these high-likelihood period-bounce candidates is presented in Sect. 4, together with a description of the necessary requirements for a confirmation, and the first successful reclassification of candidate GALEX J125751.4-283015 as a new period-bouncer. We present our conclusions in Sect. 5.

2. Selection of period-bounce candidates

In our series of papers aiming to confirm and characterize new period-bouncers (Muñoz-Giraldo et al. 2023; Muñoz-Giraldo et al. 2024a; Muñoz-Giraldo et al. 2024b), we have detected 9 known period-bouncers using eROSITA and confirmed 12 new period-bouncers through multiwavelength analysis also involving eROSITA (6 of the new period-bouncers had already been suggested as candidates in the literature). This represents a 33% increase in the population of confirmed period-bouncers, proving the usefulness of X-ray data, specifically from eROSITA, in the search for the missing population of period-bouncers.

Continuing our effort in the identification of new period-bouncers, we now search for X-ray emission from a population of *Gaia*-selected WD candidates (Gentile Fusillo et al. 2021). We then apply a reduced version of the multiwavelength period-bouncer scorecard introduced in Muñoz-Giraldo et al. (2024a) to those *Gaia* candidate WDs with a reliable eROSITA X-ray detection. This way we define high-likelihood period-bounce candidates that have multiwavelength characteristics resembling those of confirmed members of this class.

2.1. The Gaia WD candidate catalog by Gentile Fusillo et al. (2021)

We used the *Gaia* Data Release 3 (DR3) catalog of 1280266 WD candidates by Gentile Fusillo et al. (2021) as a starting point in the search for new period-bouncers. This is because in the optical band period-bouncers are very likely to appear as single WDs, especially if they are in a quiescent state, since the contribution of the highly evolved secondary in period-bouncers is expected to be negligible at optical wavelengths (Santisteban et al. 2018).

The Gentile Fusillo et al. (2021) WD catalog was compiled using *Gaia* data for spectroscopically confirmed SDSS Data Release 16 WDs to construct broad cuts in the Hertzsprung–Russell (H-R) diagram that span the entire parameter space occupied by WDs. Further selection cuts based on absolute magnitude, color, and *Gaia* quality flags were used by Gentile Fusillo et al. (2021) to remove the majority of contaminating objects. Fits of standard hydrogen atmosphere spectral models (Tremblay et al. 2011) to the *Gaia* data were then used to obtain several parameters of the WD, including effective temperature, surface gravity, and mass. For hot WDs ($T_{\rm eff} \gtrsim 50\,000$ K), *Gaia* colors have little sensitivity to effective temperatures (Carrasco et al. 2014). However, the WDs in period-bouncers are cool ($T_{\rm eff} \lesssim 12\,500$ K; Pala et al. 2022), such that the effective temperature values obtained by Gentile Fusillo et al. (2021) from *Gaia* colors should be accurate (see detailed discussion in Sect. 2.2).

For the selection of period-bounce candidates, the most relevant parameter from the Gentile Fusillo et al. (2021) catalog is the probability of being a WD ($P_{\rm WD}$). This parameter was

Table 1. Unified list of thirty-three confirmed period-bouncers including twenty-one bona fide period-bouncers.

Period-bouncer	Donor SpT	Reference	Score [%] Full	Reduced	P_{WD}	eROSITA detection
V379 Vir	L8 (S)	Farihi et al. (2008)	100	100	0.996	x
SDSS J15141+0744	L3 (P)	Breedt et al. (2012)	69	83	0.778	
PM J12507+1549	M8 (P)	Breedt et al. (2012)	67	100	0.979	x
SDSS J10575+2759	L5→ (P)	McAllister et al. (2017)	85	80	0.872	x
SDSS J14331+1011	L1 (S)	Santisteban et al. (2016)	75	61	0.951	
WZ Sge	L2 (S)	Harrison (2015)	90	100	0.986	
SDSS J10353+0551	L0→ (P)	Southworth et al. (2006)	88	87	0.996	x
SMSS J16063-1000	L2→L8 (P)	Kawka et al. (2021)	70	100	0.992	
QZ Lib	T (S)	Pala et al. (2018)	100	100	0.979	x
GD 552	L0 (S)	Unda-Sanzana et al. (2008)	79	67	0.959	
MT Com	L→ (P)	Patterson et al. (2005)	76	100	0.971	
V455 And	L2→ (P)	Araujo-Betancor et al. (2005)	88	92	0.637	
V406 Vir	L3 (S)	Pala et al. (2019)	64	72	0.979	x
BW Scl	T (S)	Neustroev & Mäntynen (2023)	82	80	0.960	x
EZ Lyn	L2 (P)	Zharikov et al. (2013)	93	100	0.991	
CRTS J12222-3115	L0→ (P)	Neustroev et al. (2017)	77	75	0.976	x
V1108 Her	L1 (S)	Ishioka et al. (2007)	81	67		
GALEX J04113+6853	T (S)	Galiullin et al. (2024)	65	75	0.986	–
HV Vir	L5 (P)	Mennickent & Diaz (2002)	61	73	0.926	x
WD J18204-0422	T5→ (P)	Cunningham et al. (2025)	79	100	0.991	
WD J19070+2052	T6→ (P)	Cunningham et al. (2025)	79	100	0.991	
LP 731-60			92	87	0.995	x
EG Cnc			89	83	0.995	x
SDSS J12160+0520			100	100	0.984	x
1RXS J02323-3718			67	83	0.984	x
WISE J11121-3538			94	89	0.839	x
PM J12192+2049			81	87	0.990	x
PNV J17144-2943			80	67	0.988	x
CRTS J10441+2113			67	73	0.965	x
SDSS J07550+1435			62	80	0.994	x
1RXS J10142+0638			92	100	0.986	x
2QZ J14283+0031			72	72	0.985	x
eRASS J05472+1326			100	100	0.984	x
CP Tuc	T→ (P)	This work	89	100	0.993	x
ASASSN -17el	L9→ (P)	This work	94	89	0.966	x
ASASSN -18fk	T→ (P)	This work	71	87	0.943	x
PM J11384+0619	T→ (P)	This work	72	72	0.968	x
Gaia 18ctg	T→ (P)	This work	80	75	0.858	x
GALEX J12575-2830	L0→ (P)	This work	72	75	0.899	x

Notes. This list was compiled from Muñoz-Giraldo et al. (2024a) and Muñoz-Giraldo et al. (2024b). We include the confirmation of a late-type donor in the system through spectroscopy (S) or photometry (P) for 21 confirmed period-bouncers (referred to as bona fide period-bouncers). The remaining 12 confirmed period-bouncers do not yet have a detected late-type donor. The score value of each system is given for: the period-bounce scorecard defined by Muñoz-Giraldo et al. (2024a) and the reduced period-bounce scorecard (see Sect. 2.2). The probability of being a WD (P_{WD}) is presented for the period-bouncers found in Gentile Fusillo et al. (2021). We indicate the period-bouncers with an eROSITA detection from the western (*x*) and eastern (-) Galactic half-sky.

calculated by Gentile Fusillo et al. (2021) for each member of the catalog using as a reference a sample of 22 998 spectroscopically confirmed WDs from SDSS and 7124 contaminants (mainly composed of stars and quasi-stellar objects). They found that about 91% of the spectroscopically confirmed WDs from SDSS are recovered when selecting objects with $P_{WD} > 0.75$ (Gentile Fusillo et al. 2021). Our match of these high-fidelity WDs ($P_{WD} > 0.75$) with the list of confirmed period-bouncers reported in Table 1 results in 94% of them being recovered. These high-fidelity WDs are therefore an ideal starting sample for a search for new period-bouncers. In Fig. 1 we show the high-fidelity WD sample from Gentile Fusillo et al. (2021) that populates the WD locus and area surrounding it, and we highlight the 31 confirmed period-bouncers included in this sample.

The search for period-bouncers, which are known for exhibiting very low mass accretion rates and therefore constituting the faintest CVs, should be distance-limited in order to be effective. Motivated by the eRASS sensitivity limit and the reduced accuracy in *Gaia* distance measurements achieved for faint objects (see Muñoz-Giraldo et al. 2024a for more details), we enforce a distance limit of 500 pc for the high-fidelity WDs (see Fig. 1), and thus narrow down the sample to 246731 *Gaia* objects that resemble spectroscopically confirmed WDs in the optical band.

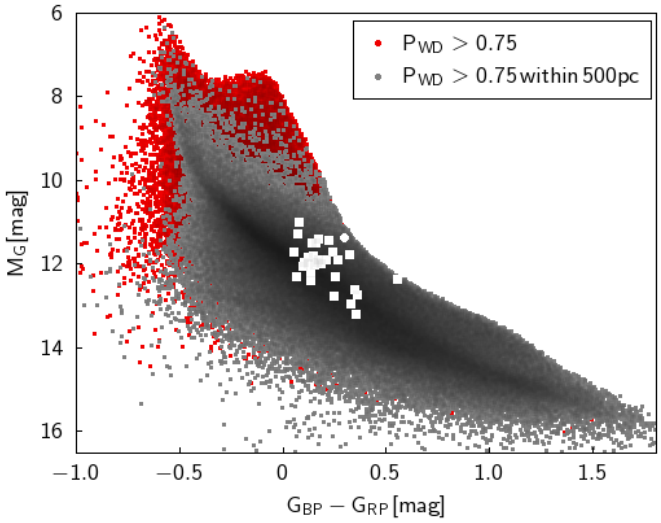

Fig. 1. Population of high-fidelity WDs from Gentile Fusillo et al. (2021) with the confirmed period-bouncers in this population (white squares). The only confirmed period-bouncer with a distance larger than 500 pc is highlighted as a circle.

2.2. A reduced version of the period-bouncer scorecard

Our period-bouncer scorecard, first introduced by Muñoz-Giraldo et al. (2024a), is composed of ten parameters that were constructed following defined characteristics for an ideal period-bouncer found in the literature: spectral type of the donor (Knigge et al. 2011, Kirkpatrick & McCarthy 1994), donor mass (Knigge et al. 2011), orbital period (Gänsicke et al. 2009), WD temperature (Pala et al. 2022), *Gaia* variability (Inight et al. 2023a), *Gaia* colors (Jiménez-Esteban et al. 2018, Gentile Fusillo et al. 2021), SDSS colors (Inight et al. 2023a), ultraviolet colors (Patterson 2011), infrared colors (Littlefair et al. 2003), and infrared excess (Girven et al. 2011, Owens et al. 2023). The application of the period-bouncer scorecard to our catalog of known CVs around the period-bounce made up of 217 systems proved the usefulness of this tool as it produced a list of 76 high-likelihood period-bouncer candidates, of which 12 were successfully confirmed (Muñoz-Giraldo et al. 2024a, Muñoz-Giraldo et al. 2024b) thanks to the use of two additional X-ray parameters based on the eROSITA X-ray luminosity and X-ray-to-optical flux ratio of "bona fide" period-bouncers.

The scores of the period-bouncers allow us to establish the performance of each parameter in the scorecard using its "completeness" and "accuracy". Here, completeness refers to the percentage of confirmed period-bouncers (Table 1) that obtain the highest score for the parameter, quantifying how many confirmed period-bouncers resemble characteristics of an ideal period-bouncer from the literature. Accuracy refers to the percentage of systems with the highest score for the parameter that are confirmed period-bouncers, measuring the "contamination" from non-period-bouncers. The values for completeness and accuracy are given in Table 2 for all ten parameters from the scorecard.

Overall, the values for the completeness show that the characteristics for an ideal period-bouncer from the literature describe around half or more of the actual population of confirmed period-bouncers. The accuracy, on the other hand, shows that the characteristics for an ideal period-bouncer from the literature (with the exception of the spectral type of the donor) also apply to a considerable number of systems that have not been confirmed as period-bouncers. This suggests that there are systems among the "contaminants" that might be part of the missing population of period-bouncers.

The parameter with the highest accuracy is the "spectral type of the donor". This is not unexpected, considering that a spectroscopic detection of a late-type donor in a CV is the ultimate confirmation that the system is a period-bouncer. However, the completeness of this parameter is only around 40%, mainly due to the lack of a spectroscopic confirmation of the very late-type donor in several confirmed period-bouncers (see Table 1). "Ultraviolet colors" is the only other parameter with an accuracy higher than 50%, with 53% of systems that fulfill this selection cut being confirmed period-bouncers. The parameter that performs the best overall is "*Gaia* colors", as it manages to retrieve 83% of confirmed period-bouncers while also selecting among the fewest "contaminants". According to this, it is likely that a CV with *Gaia* colors locating it within the selection cuts presented in the scorecard, is indeed a period-bouncer. This is especially useful considering that *Gaia* colors are easily available (retrieved for 76% of our known CVs around the period-bounce), which is not the case for the spectral type of the donor (retrieved for 20% of our known CVs around the period-bounce).

These diagnostics allowed us to identify which parameters recover the majority of already confirmed period bouncers (high completeness in Table 2) while simultaneously identifying candidates that are actual period bouncers (high accuracy in Table 2), providing a robust basis for classification. In particular, the most useful and relevant parameters for assessing whether a CV is a period-bouncer are: the donor spectral type, *Gaia* colors, and ultraviolet colors.

Because the scorecard will be applied to a population of objects that have been published in the Gentile Fusillo et al. (2021) WD catalog as single objects, we do not have available information for the first three parameters (spectral type of donor, donor mass, and orbital period) for a significant number of objects, as they correspond to parameters relating to the system being a binary. Therefore, we define a reduced version of the period-bouncer scorecard that is composed of the remaining seven parameters that mostly rely on multiwavelength photometry: WD temperature, *Gaia* variability, *Gaia* colors, SDSS colors, UV colors, IR colors, and IR excess.

For the reduced version of the period-bounce scorecard, we exclusively use the WD temperature reported in the Gentile Fusillo et al. (2021) catalog derived from *Gaia* photometry, assuming that it represents the WD temperature of a period-bouncer in quiescence and not in an outburst. Out of the confirmed period-bouncers found among the high-fidelity WDs, 21 have reliable WD temperatures in quiescence determined previously in the literature through a detailed study, which can be compared to their respective WD temperatures reported by Gentile Fusillo et al. (2021). As can be seen in Fig. 2 (left panel), 14 of 21 confirmed period-bouncers have a WD temperature reported by Gentile Fusillo et al. (2021) within 20% of the value reported previously in the literature. This figure also shows that the sensitivity of *Gaia* color to WD temperature decreases as the latter increases (Carrasco et al. 2014), with the reliability of *Gaia* derived WD temperatures falling particularly for values greater than 12 500 K. Additionally, the confirmed period-bouncers with the smallest difference between their WD temperature values are located mainly in the area after the period-bounce (see Fig. 2 right panel), which indicates that using the WD temperature reported in the Gentile Fusillo et al. (2021) WD catalog is reliable especially for evolved period-bouncers;

Table 2. Completeness and accuracy when applied to a population of 219 known CVs around the period-bounce.

	Donor					Color				
	SpT	Mass	Orbital period	WD temperature	*Gaia* variability	Gaia	SDSS	UV	IR	IR excess
Completeness	43	56	57	70	97	84	81	43	53	93
Accuracy	90	25	25	37	29	47	21	53	45	25

Notes. Numbers represent percentages.

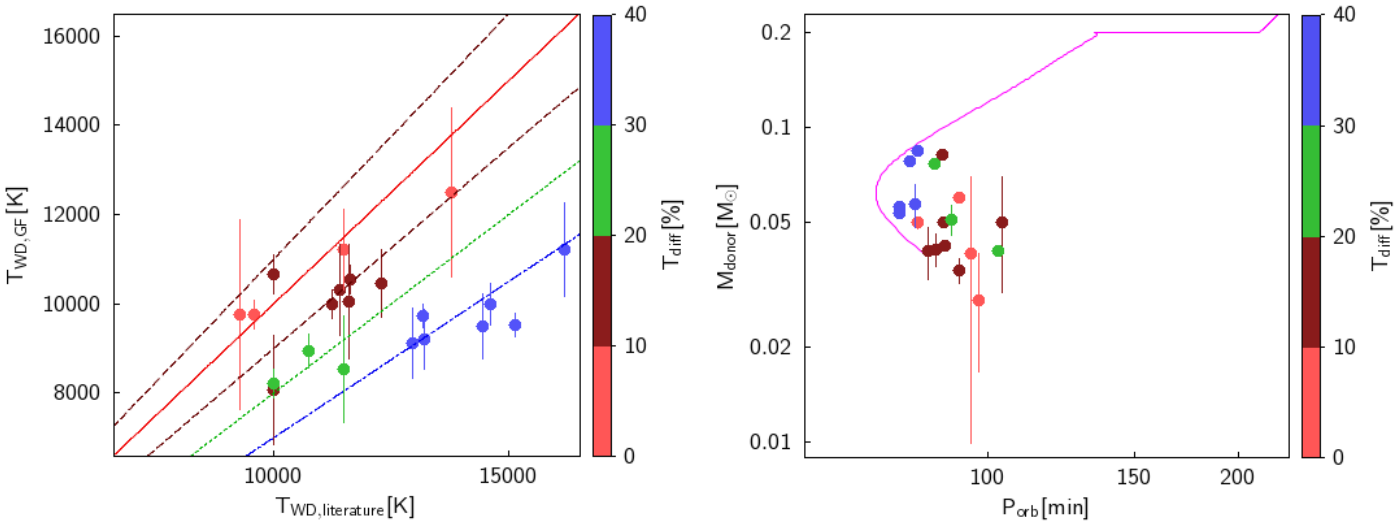

Fig. 2. *Left panel:* Comparison between WD temperatures obtained from individual literature studies versus those of the Gentile Fusillo et al. (2021) WD catalog. Values from the WD catalog that agree within the uncertainties with the literature values are shown in light red. We also show differences between these values of less than 10% (in brown), between 10% and 20% (in green), and more than 20% (in blue). *Right panel:* Orbital period versus donor mass. Standard evolution track for CVs (Knigge et al. 2011) is shown in pink as a reference.

that is, those with periods longer than the nominal period minimum.

The final score was then calculated considering only the seven parameters from the reduced scorecard. We are confident that the results from the reduced scorecard are reliable as it includes two of the three best performing parameters, *Gaia* and ultraviolet colors. Apart from the spectral type of the donor, these are the most relevant parameters for the identification of period-bouncers (see Table 2 and discussion above).

In Table 1, we show the final reduced scores for the confirmed period-bouncers calculated using the value reported by Gentile Fusillo et al. (2021) for the WD temperature. We see three tendencies among the confirmed period-bouncers: (1) systems for which the score does not change significantly when using the full or reduced scorecard, indicating that both the multiwavelength photometry and the binary parameters obtained for them are consistent with a classification as a period-bouncer; (2) systems for which the reduced score increases compared to the full score, meaning that these systems have binary parameters in the pre-bounce area inconsistent with the period-bouncer status suggested by their multiwavelength photometry. At least two of these systems have uncertain donor mass determinations that cause this lower full value for the score (SDSS J151415.65+074446.4 and PM J12507+1549; Breedt et al. 2012); (3) systems for which the reduced scores decreases compared to the full score. These are systems with multiwavelength photometry that falls outside the expectations for period-bouncers, and the strongest reason to be classified as period-bouncers is their securely determined binary parameters.

3. eROSITA data

Between December 2019 and December 2021, eROSITA carried out four full-sky surveys, correspondingly named eRASS 1 to eRASS 4 (Merloni et al. 2024). Source catalogs from eRASS data are produced at Max Planck Institut für extraterrestrische Physik (MPE) in Garching, Germany, with the eROSITA Science Analysis Software System (eSASS) described by Brunner et al. (2022). These catalogs comprise all eRASS sources in the western half of the sky in terms of Galactic coordinates (Galactic longitude $l \geq 180°$), which is the sky area with German data rights on the eROSITA observations. From the list of 246731 high-fidelity WDs within 500 pc, 124657 are located in the area with German data rights.

To obtain the highest sensitivity for detecting the presumably faint period-bouncers hiding in the Gentile Fusillo et al. (2021) WD catalog, we used the merged catalog eRASS:4, which was generated from summing data from the first four all-sky surveys. The version of the eRASS:4 catalog used was produced with the data processing version 020[1]. Source detection was performed in this catalog for three energy bands: 0.2–0.6 keV (soft band), 0.6–2.3 keV (medium band), and 2.3–5.0 keV (hard band).

3.1. Gaia WDs with eROSITA counterparts

We corrected the coordinates of the Gentile Fusillo et al. (2021) WD catalog to the mean observing date of eRASS:4 using the individual *Gaia* DR3 proper motions of the systems. We

[1] The source catalog used in our work is all_s4_SourceCat3B_221031_poscorr_mpe_clean.fits (for eRASS:4).

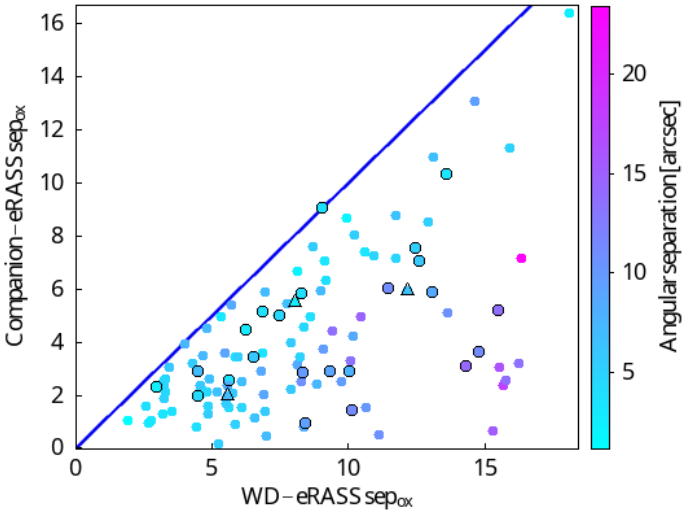

Fig. 3. Comparison of the separations between the optical and Xray source of the *Gaia* DR3 WD from Gentile Fusillo et al. (2021) versus the companion in a possible resolved binary. The angular separation between the components of the possible resolved binary is shown as a color scale. We highlight with black circles the known WD-MS wide binaries and with black triangles the WD-WD wide binaries (El-Badry & Rix 2018).

then used the corrected coordinates to produce a match with the eRASS:4 catalog, allowing for a maximum separation of $\mathrm{sep_{ox}} = 30''$, and enforcing the condition $\mathrm{sep_{ox}} < 3 \times RADEC\_ERR$, where $RADEC\_ERR$ is the positional error of the X-ray coordinates in units of arcseconds. We also checked that the eROSITA counterpart corresponds to a point source ($EXT = 0$ in the eRASS catalogs). This way we found that 912 of the 124657 high-fidelity WDs within 500 pc located in the area with German data rights are detected in the eRASS:4 catalog, referred to from this point on as the "eROSITA WD subsample". Performing a reverse match between the eRASS:4 counterpart and the *Gaia* DR3 catalog, allowing for a maximum separation of 30″, we obtain that for 601 members of the eROSITA WD subsample the closest *Gaia* DR3 source to the eRASS:4 source corresponds to the *Gaia* DR3 WD from Gentile Fusillo et al. (2021). We therefore consider these 601 *Gaia* DR3 WDs to have an X-ray counterpart. This includes 122 possible resolved binaries revealed by similar *Gaia* parallaxes and proper motions (24 are known WD-MS wide binaries and 4 are known WD-WD wide binaries from El-Badry & Rix 2018). The remaining 311 members have another *Gaia* DR3 source closer to the eRASS:4 source such that the identification with the *Gaia* DR3 WD from Gentile Fusillo et al. (2021) is uncertain. These should be examined in a case-by-case basis.

In Fig. 3 we show for the 122 possible resolved binaries the difference in separations between the eRASS:4 source and either the *Gaia* DR3 WD from Gentile Fusillo et al. (2021) or the possible companion. Even though all of these possible resolved binaries were identified due to another *Gaia* source being closer to the eRASS:4 source, for more than half of them the *Gaia* DR3 WD from Gentile Fusillo et al. (2021) is only at a slightly larger separation, increasing the likelihood that the X-ray emission is coming from the WD and not the possible companion.

The systems in the eROSITA WD subsample with an X-ray counterpart thus comprise only 0.48% of the high-fidelity WDs within 500 pc. This is most likely because the majority of them are indeed single WDs that produce faint X-rays below the eROSITA sensitivity limit or no X-rays at all.

Table 3. Rate-to-flux conversion factors for each eROSITA energy band.

	Soft band 0.2–0.6 keV	Medium band 0.6–2.3 keV	Hard band 2.3–5.0 keV
$CF_{\mathrm{fake,powerlaw}}$	3.61×10^{11}	4.61×10^{11}	3.33×10^{10}
$CF_{\mathrm{fake,APEC}}$	3.97×10^{11}	4.58×10^{11}	3.57×10^{10}

Notes. In units of cts cm^2 erg^{-1}. Conversion factors were calculated for simulated spectra obtained using an APEC model and a power law model with parameters detailed in Sect. 3.1.

The eROSITA catalog holds the flux for a power law model with an index of $\Gamma = 2.0$ and a galactic absorption of $N_{\mathrm{H}} = 3 \times 10^{20}\,\mathrm{cm}^{-2}$ (Brunner et al. 2022). Since this spectral model is not appropriate for CVs, which are characterized by a thermal plasma, we computed fluxes for an APEC model, following the procedure detailed by Muñoz-Giraldo et al. (2023), with the help of a simulation that provided us with the eROSITA conversion factor, from count rate to thermal flux. We used an APEC model with $kT = 2.62$ keV, $N_{\mathrm{H}} = 2.3 \times 10^{20}\,\mathrm{cm}^{-2}$ and an abundance of $0.11\,Z_{\odot}$, which are the values found from the *XMM-Newton* spectrum for one of the eROSITA-detected bona fide period-bouncers (see Stelzer et al. 2017). In Table 3 we compare both conversion factors obtained using the simulation for a power law model ($CF_{\mathrm{fake,powerlaw}}$) and for an APEC model ($CF_{\mathrm{fake,APEC}}$) specifically for the eRASS:4 catalog (the values presented in Muñoz-Giraldo et al. 2023 were obtained for a single-band eRASS:3 catalog), where it can be seen that these CFs differ by at most 10%. This result allowed us to derive the $CF_{\mathrm{eROSITA,APEC}}$ from the $CF_{\mathrm{eROSITA,powerlaw}}$ used in the eRASS:4 catalog.

The final values for the APEC fluxes for each eROSITA band (0.2–0.6 keV soft band, 0.6–2.3 keV medium band, and 2.3–5.0 keV hard band) were calculated using the eRASS:4 catalog count rate and the APEC eROSITA conversion factor as $Flux_{\mathrm{APEC,i}} = R_i / CF_{\mathrm{eROSITA,APEC}}$, where i = S,M,H and R_i is the count rate in each band. The total APEC flux was calculated as the sum of the individual APEC fluxes from each band. We combined the total APEC flux with the distance reported in the Gentile Fusillo et al. (2021) catalog to calculate the X-ray luminosity of each object.

3.2. X-ray selection cuts

Following our earlier work (Muñoz-Giraldo et al. 2024a), we used diagnostic diagrams that combine X-ray and optical data to establish selection cuts for period-bounce candidates based on the parameter space occupied by bona fide period-bouncers. Because the number of bona fide period-bouncers detected in each eROSITA catalog can vary, the X-ray selection cuts derived by Muñoz-Giraldo et al. (2024a) for eRASS:3 are not necessarily applicable to eRASS:4. In Figs. 4 and 5 we have placed the eROSITA WD subsample in two diagnostic diagrams comprising eRASS data: X-ray-to-optical flux ratio ($\mathrm{F_x}/F_{\mathrm{opt}}$) and X-ray luminosity ($\mathrm{L}_x$) versus *Gaia* color. The position of the eROSITA WD subsample is compared with the eROSITA-detected confirmed period-bouncers.

In Fig. 4 more than half of the eROSITA WD subsample displays $-1 \leq \log(\mathrm{F_x}/\mathrm{F_{opt}}) \leq 0$, typical of systems with a low mass transfer rate including different CV types such as

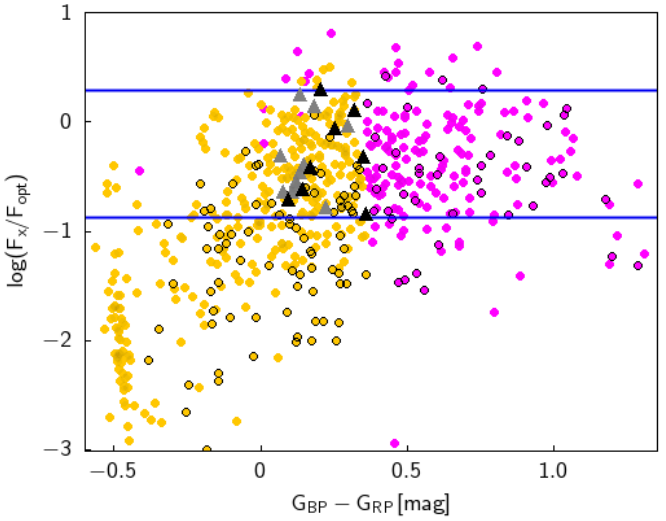

Fig. 4. X-ray-to-optical flux ratio as a function of *Gaia* colors showing the position of the eROSITA WD subsample (circles) and confirmed period-bouncers (triangles) detected in eRASS:4. The bona fide period-bouncers used to establish the selection cuts are highlighted in black. See text for the justification of the selection cut lines. The members of the eROSITA WD subsample that fulfill the X-ray luminosity and *Gaia* colors selection cuts are highlighted in yellow; the ones that do not are in pink. Black circles are placed around possible resolved binaries in the eROSITA WD subsample.

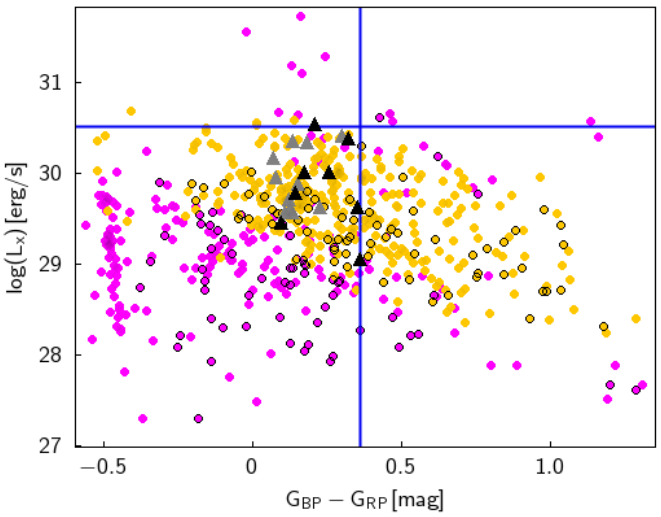

Fig. 5. Bolometric X-ray luminosity as a function of *Gaia* colors showing the position of the eROSITA WD subsample (circles) and the bona fide period-bouncers (triangles) detected in eRASS:4. The bona fide period-bouncers used to establish the selection cuts are highlighted in black. See text for the justification of the selection cut lines. The members of the eROSITA WD subsample that fulfill the X-ray-to-optical flux ratio selection cut are highlighted in yellow; the ones that do not are in pink. Black circles are placed around possible resolved binaries in the eROSITA WD subsample.

dwarf novae, polars, and intermediate polars (Schwope et al. 2024). This parameter on its own does not identify potential period-bouncers, but it serves to discard systems with high optical flux indicative of either high-mass-transfer-rate CVs or hot single WDs. The members of the eROSITA WD subsample accumulating toward the bottom left corner of Fig. 4 all have WD temperatures reported by Gentile Fusillo et al. (2021) hotter than 25 000 K, more than twice the expected value for period-bouncers, with 34 of them already being securely identified as single WDs (Friedrich et al. 2025).

In Fig. 5 almost all of the eROSITA WD subsample displays $L_x \leq 10^{31}$ erg/s, characteristic of period-bouncers and low-mass transfer systems. The eROSITA WD subsample shows a broad distribution in *Gaia* color, which, excluding the distinct group around $G_{BP} - G_{RP} \cong -0.5$ discussed above, represents systems dominated by cool WDs with effective temperatures between 7000 K and 15 000 K.

X-ray plus *Gaia* color selection cuts (see blue lines in Figs. 4 and 5) are defined on the basis of the position of eROSITA-detected bona fide period-bouncers in Figs. 4 and 5 as discussed above, and are shown as blue lines resulting in upper and lower limits for the X-ray-to-optical flux ratio ($-0.87 \leq \log(F_x/F_{opt}) \leq 0.28$), and in upper limits for the X-ray luminosity ($\log(L_x) \leq 30.52$ [erg/s]) and *Gaia* color ($G_{BP} - G_{RP} \leq 0.36$). These three criteria are fulfilled by 213 members of the eROSITA WD subsample, which are henceforth considered period-bounce candidates.

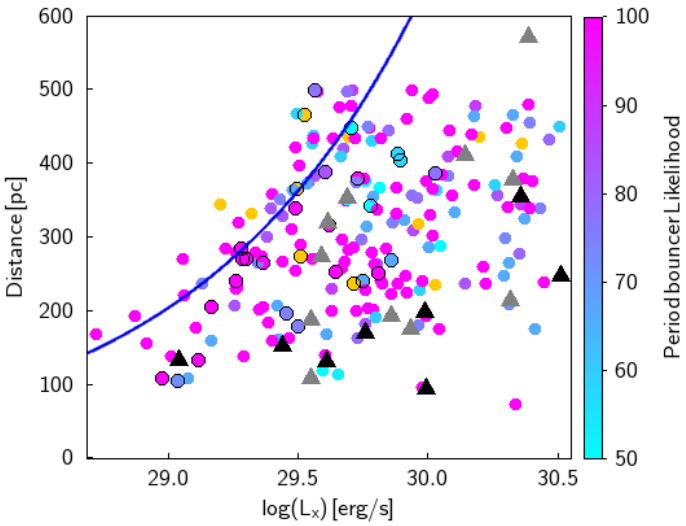

Fig. 6. Distance from Bailer-Jones et al. (2021) versus X-ray luminosity showing the position of the 213 period-bounce candidates (in color scale) and the eROSITA-detected confirmed period-bouncers (in triangles, bona fide period-bouncers are highlighted in black). The average eRASS:4 sensitivity limit is marked by the blue line (see text in Sect. 4). Black borders are used to show possible resolved binaries in the eROSITA WD subsample.

4. High-likelihood period-bounce candidates

We show in Fig. 6 the relationship between X-ray luminosity and distance for the period-bounce candidates identified in Sect. 3.2. Using a conservative eRASS:4 detection likelihood of DET_ML > 10, which corresponds to the value for 2QZ J14283+0031 (the lowest among eROSITA-detected confirmed period-bouncers), 95% of the sources in the full eRASS:4 catalog have a flux higher than 2×10^{-14} erg/cm^2/s, which is used to calculate the average eRASS:4 sensitivity limit shown in Fig. 6 as a blue line. Our new period-bounce candidates tend to have, at a given distance, even lower X-ray luminosity when compared to eROSITA-detected confirmed period-bouncers. X-ray faint sources are of special interest in our search for period-bouncers considering that they might have remained undetected

in other multiwavelength searches for the missing members of this population.

To test whether the 213 period-bounce candidates, especially the ones around the eRASS:4 sensitivity limit, constitute the missing population of period-bouncers, we applied the reduced scorecard introduced in Sect. 2.2 to this population. The calculated final scores are presented as a color scale in Fig. 6. Period-bounce candidates that have reported values only for two or fewer of the parameters from the reduced scorecard do not have enough information for us to accurately judge their status as a period-bouncer and therefore are not assigned a final score (yellow symbols in Fig. 6).

The eROSITA-detected bona fide period-bouncer with the lowest final score calculated using the reduced scorecard is V406 Vir (also the lowest scoring bona fide period-bouncer in Muñoz-Giraldo et al. 2024a and Muñoz-Giraldo et al. 2024b) with a reduced final score of 72%. This means that a category of high-likelihood period-bouncers can be defined as systems that have final scores higher than this value. This applies to 161 systems that we consider to be high-likelihood period-bounce candidates. It is relevant to mention that a high fraction of these high-likelihood period-bounce candidates, 108 systems, have a final score of 100% according to the reduced scorecard (systems shown in pink in Fig. 6).

4.1. Classification

A crossmatch with SIMBAD gives us the classification of the 161 high-likelihood period-bounce candidates according to the previous literature. The J2000 coordinates (given in epoch 2016.0) available from the *Gaia* DR3 catalog were used for a crossmatch with SIMBAD[2]. We verified that the object retrieved from the match had the same *Gaia* DR3 SOURCE_ID as the one reported in the Gentile Fusillo et al. (2021) catalog. Here we give more information on the SIMBAD classification:

Period-bouncers: Fifteen of the high-likelihood period-bounce candidates are already known systems classified as period-bouncers, including six eROSITA-detected bona fide period-bouncers and nine eROSITA-confirmed period-bouncers. The successful retrieval of these systems from the Gentile Fusillo et al. (2021) WD catalog conclusively proves the usefulness of our selection tools (period-bouncer scorecard and X-ray selection cuts) in identifying period-bouncers hiding in WD catalogs.

Cataclysmic variables: Five of the high-likelihood period-bounce candidates had already been classified as CVs. This includes one known polar (CP Tuc; Thomas & Reinsch 1996), one known WZ Sge (ASSASN -17el; vsnet-alert 20866), one known nova (ASASSN -18fk; vsnet-alert 21992), and two without further classification (PM J11384+0619; Szkody et al. 2006 and Gaia 18ctg; Hodgkin et al. 2021). ASASSN -17el is the only system that is included in the catalog of CVs around the period-bounce by Muñoz-Giraldo et al. (2024a) and was initially not confirmed as a period-bouncer due to its X-ray luminosity in eRASS:3 being slightly higher than the X-ray selection cut used; however, considering that it falls within the selection cut for eRASS:4 we can now confirm it as a new period-bouncer. The other four systems were not included in the catalog of CVs around the period-bounce by Muñoz-Giraldo et al. (2024a) or its update (Muñoz-Giraldo et al. 2024b) as they had not previously been suggested as period-bouncers and did not have an orbital period or donor mass placing them in the period-bounce area. We hereby confirm all four of these systems (CP Tuc, ASASSN -18fk, PM J11384+0619, and Gaia 18ctg) as new period-bouncers considering that they have an IR excess and multiwavelength colors (GALEX, SDSS and IR) in addition to their eROSITA and *Gaia* data that support their classification as period-bouncers, as well as photometrically detected very late-type donors (see Appendix A).

AM CVn binaries: Two of the high-likelihood period-bounce candidates are already known AM CVn binaries (V396 Hya; GP Com). This is a distinct subclass of CVs that underwent CE evolution twice, rather than the single CE evolution that the rest of the CVs undergo (Nelemans et al. 2001). AM CVn binaries are known for containing a WD accreting from a hydrogen-deficient donor star that is fully or partially degenerate (Deloye et al. 2005). They exhibit orbital periods from 5 min to 68 min (Levitan et al. 2015, Ramsay et al. 2018, Green et al. 2020). Similar to period-bouncers, AM CVn binaries are heavily underrepresented in observational surveys for CVs (Rodriguez et al. 2025). From this result, we can anticipate that a small number of our high-likelihood period-bounce candidates will turn out to be AM CVn binaries, meaning that our search will also contribute to the characterization of another underrepresented population.

RR Lyrae Variable Candidate: One of the high-likelihood period-bounce candidates has been tentatively identified as a RR Lyr variable candidate based on its *Gaia* data (Gaia DR3 2930889294867085440; Clementini et al. 2019). Because there is no additional information on this system apart from eROSITA and *Gaia* data, we cannot securely classify it as a CV or a period-bouncer. Follow-up of this target is required to proceed with its confirmation as a period-bouncer.

WDs and WD candidates: The remaining 138 high-likelihood period-bounce candidates are classified as either WDs or WD candidates, with ∼80% of them only appearing in the literature as part of large WD catalogs (Jiménez-Esteban et al. 2018, Gentile Fusillo et al. 2019, Gentile Fusillo et al. 2021, Torres et al. 2023, Vincent et al. 2024). One confirmed period-bouncer (eRASS J05472+1326; Rodriguez et al. 2025) is incorrectly classified as a WD in SIMBAD, such that we do not need to consider it further in our effort to confirm new period-bouncers. These candidates constitute the focus of the following sections.

4.2. Confirmation of high-likelihood period-bounce candidates

We are left with 137 high-likelihood period-bounce candidates that are classified as WDs or WD candidates. The confirmation of these candidates is imperative for the discovery of the missing population of period-bouncers. Here we describe what are the required steps for a secure period-bouncer classification, followed by the presentation of a newly identified period-bouncer using this approach.

[2] SIMBAD stands for Set of Identifications, Measurements and Bibliography for Astronomical Data, available at http://simbad.cds.unistra.fr/simbad

4.2.1. Requirements for confirmation as a period-bouncer

In order to securely confirm the 137 high-likelihood candidates classified as WDs or WD candidates as period-bouncers we should fulfill three requirements: confirmation of the system as a CV, determination of an orbital period, and detection of a late-type donor.

Confirmation as a CV: In order to confirm a system as a period-bouncer, we must first make sure that it is a CV, meaning that it is an interacting or accreting binary rather than a single WD. The most straightforward method to do so is through the detection of Balmer emission lines in the optical spectra of potential CV candidates (Warner 1995), which is a clear indicator of accretion in the system, and conclusively differentiates them from single WDs that only present Balmer absorption lines (Wesemael et al. 1993). The SDSS-V Project is pioneering all-sky panoptic[3] spectroscopy by providing the first optical plus infrared survey for millions of sources spread across the entire sky (Kollmeier et al. 2019, 2025). One of the SDSS-V subprojects aims to spectroscopically observe up to 60 000 WDs. The survey began its run in November 2020, initially using the 2.5 m telescope at the Apache Point Observatory (Gunn et al. 2006), and has now expanded to the 2.5 m telescope at Las Campanas Observatory (Bowen & Vaughan 1973). It observes targets using the Baryon Oscillation Spectroscopic Survey spectrograph (BOSS; Smee et al. 2013) and the Apache Point Observatory Galactic Evolution Experiment spectrographs (APOGEE; Wilson et al. 2019). Most of the WDs are observed as part of the multi-epoch Milky Way Mapper program (MWM; Kollmeier et al. 2025). Each SDSS-V BOSS sub-exposure takes 900s, has a median resolution of $R \sim 1800$, and covers the wavelength range from 3600–10 000 Å. These SDSS follow-up spectra will help us confirm or deny the classification of our high-likelihood candidates as CVs, as well as help us establish if the WD is magnetic and parameters such as the WD temperature, mass, and radius (see Appendix B). Similar searches for CVs and period-bouncers, focused only on optical wavelengths, have been conducted using SDSS (Inight et al. 2023a, Inight et al. 2023b), which has led to the discovery of a large number of new systems.

Orbital period determination: The period-bounce candidate has to present an orbital modulation associated with a close interacting binary, which places the system around the period minimum of CVs (~80 min; Gänsicke et al. 2009). In Hernández-Díaz et al. (2025) we demonstrated that the two-minute cadence light curves from the *Transiting Exoplanet Survey Satellite* (TESS; Ricker et al. 2015) are well suited for efficiently detecting orbital periods of CVs. We validated the effectiveness of our methodology and introduced a probabilistic framework to assess the reliability of period detections with TESS using the parameter S/N_{PSD}, the signal-to-noise ratio (S/N) of the frequency peak in the power spectral density (PSD) corresponding to the orbital period. Our approach, which involves four different techniques to measure orbital periods, can now be applied to any other sample of CV candidates that have TESS two-minute cadence light curves available.

Detection of late-type donor: The defining characteristic of period-bouncers is the presence of a very late-type degenerate donor, which ultimately is what distinguishes them from other CVs. The detection of a very late-type donor can be achieved spectroscopically or photometrically. A spectroscopic detection results in the direct detection of the donor through observation of specific absorption lines, with a secure determination of the spectral type of the donor. On the other hand, a photometric detection or inference results in an approximation to the spectral type of the donor based on the IR excess presented by the candidate in its spectral energy distribution (SED), such that the lack of a large IR excess suggests a late-type donor. This photometric approximation of the donor SpT should be taken with caution considering that the IR excess can also be attributed to contributions from the accretion disk when the system is nonmagnetic and cyclotron emission when the system is magnetic, meaning that the actual spectral type of the donor might be later than inferred with photometry. As is detailed by Muñoz-Giraldo et al. (2024a), a spectroscopic detection of a very late-type donor is the ultimate confirmation of a CV as a period-bouncer, with a photometric detection or inference only used as definitive confirmation when other evidence supports the classification of the system as a period-bouncer.

4.2.2. GALEX J125751.4-283015: A new period-bouncer

In a preliminary, not yet systematic study following the three-fold strategy outlined in Sect. 4.2.1, we identify GALEX J125751.4-283015 as a new period-bouncer based on its SED, optical light curve, and spectrum. GALEX J125751.4-283015 is classified according to SIMBAD as a WD candidate. It has been suggested as the probable progenitor of ASASSN -18su (Barba 2018), a bright transient classified as a nonmagnetic CV (Le Guillou et al. 2015) thanks to an optical spectrum obtained with the NTT/EFOSC2 (New Technology Telescope/ESO Faint Object Spectrograph and Camera v.2).

Two optical spectra of GALEX J125751.4-283015 were obtained in the framework of the SDSS-V follow-up program outlined in Sect. 4.2.1. The SDSS spectra further supports the classification as a CV (see Fig. A.1 upper left panel) showing clear Balmer emission lines characteristic of accreting binaries. As is typical of quiescent dwarf novae, the strong Balmer emission lines are accompanied by emission of Paschen lines, He I, Ca II, and Fe II (Mason & Howell 2005, Southworth et al. 2009). In particular, the Balmer emission lines exhibit a clear double-peaked profile, arising from the Keplerian velocity distribution of the gas in the accretion disk (Smak 1969, 1982, Horne & Marsh 1986) (see Appendix C). Each of the two SDSS spectra were combined with the GALEX photometry in order to derive the WD parameters (see Appendix B), resulting in an effective temperature of between 12 000 K to 12 500 K and a $\log(g)$ of between 8.0 and 8.5, which are typical ranges for CVs near the period minimum (Pala et al. 2020, 2022). We also obtained a WD radius of between 8.01×10^8 cm and 8.93×10^8 cm that, when using the mass-radius relation by Nauenberg (1972), results in a WD mass of between 0.67 $M_\odot$ and 0.57 $M_\odot$ respectively.

GALEX J125751.4-283015 has the identifier TIC 999085360 in the TESS Input Catalog (Paegert et al. 2022), with two TESS two-minute cadence light curves, from sectors 37 and 64, available from the Barbara A. Mikulski Archive for Space Telescopes (MAST)[4]. These light curves were used to derive an orbital period of 82.17 ± 0.63.

[3] Panoptic: presenting a comprehensive or encompassing view of the whole.

[4] Space Telescope Science Institute (2024).

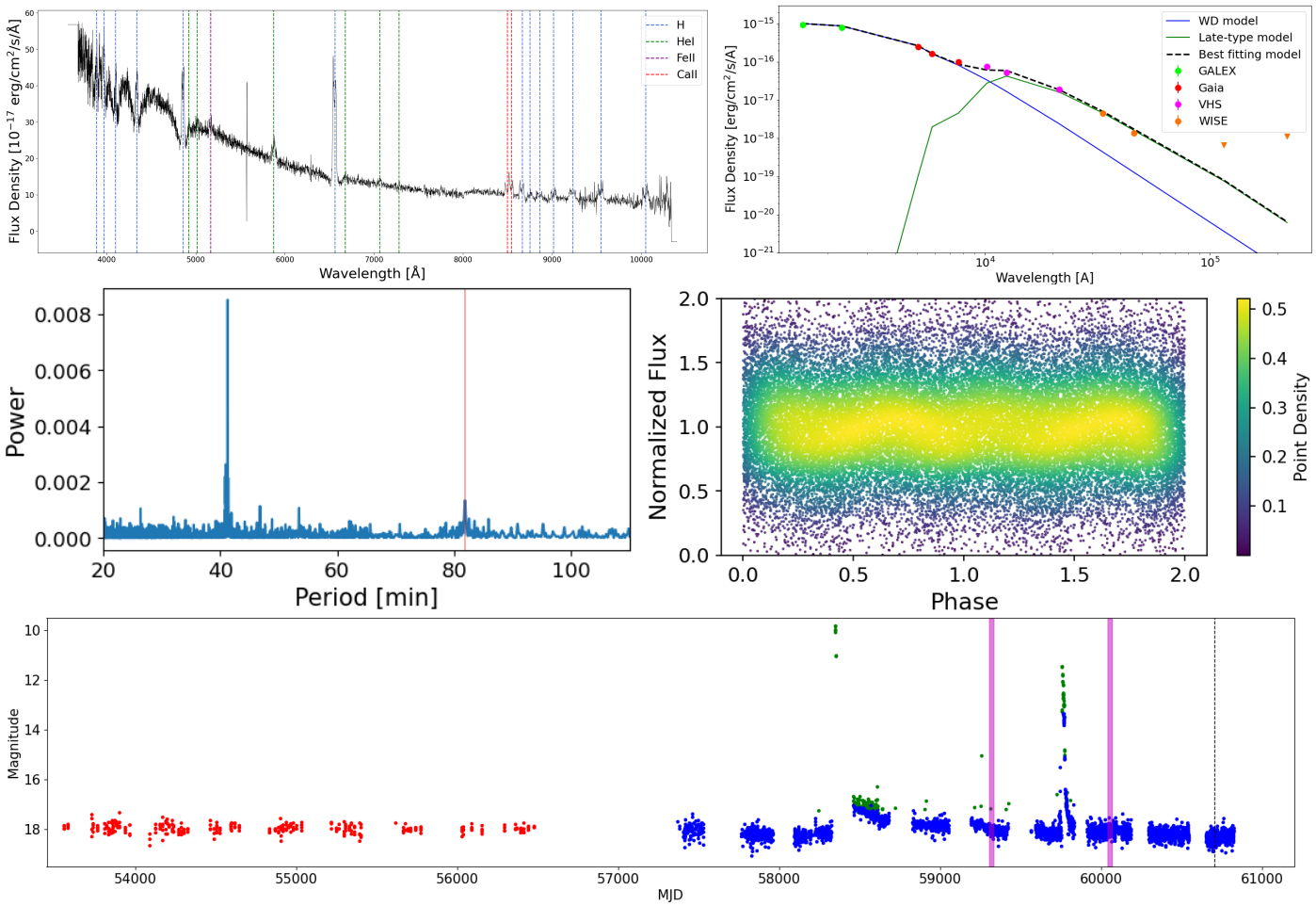

Fig. 7. Newly confirmed period-bouncer GALEX J125751.4-283015. *Upper left panel:* SDSS spectrum showing clear Balmer emission lines. *Upper right panel:* Spectral energy distribution fit using a hydrogen WD model (T_{eff} = 12 000 K and log(g) = 8.0) and a late-type star model (T_{eff} = 2000 K and log(g) = 4.5). *Middle left panel:* Peaks obtained for orbital period and half orbital period. *Middle right panel:* Phase-folded light curve (sector 64) for a period of 82.5258 min. *Lower panel:* Combined light curves from CRTS (red), ATLAS (blue), and ASAS-SN (green). Vertical purple stripes show the epochs of the TESS Sector 37 and Sector 64 light curves, while the vertical dashed black line shows the epoch of the SDSS spectrum.

In the Lomb-Scargle periodogram of the TESS two-minute cadence light curve from sector 64 (middle panels in Fig. A.1), two significant frequency peaks can be identified at 41.26 min and 81.83 min, while in the TESS two-minute cadence light curve from sector 37, only a signal at 41.26 min is detected. The signal at 41.26 min in sector 64 shows the highest significance with S/N_{PSD} = 0.011, followed by the detections at 81.83 min in sector 64 and at 41.26 min in sector 37 that have S/N_{PSD} = 0.0078 and S/N_{PSD} = 0.0077, respectively. All these values exceed the detection threshold of $(S/N_{PSD})_{min}$ = 0.004 established by Hernández-Díaz et al. (2025), supporting the reliability of these detections.

We interpret the 41.26 min signal as the second harmonic, and associate the 81.83 min signal with the orbital period. Double-humped modulations in nonmagnetic CVs can arise from the ellipsoidal modulation of the secondary (see Wilson 2006 and Bochkarev et al. 1979), from partial eclipses between the accretion disk and the secondary in high-inclination systems (see Froning et al. 1999) or from variations in the projected area of an elongated hotspot that remains visible throughout the whole orbital cycle (expected when the disk is optically thin and the hotspot optically thick), producing two brightness maxima per orbit (see e.g., Skidmore et al. 2000). In addition, the 2:1 resonance radius of the disk (see Kunze & Speith 2005) can drive two spiral density waves in its outer ring, also producing a double-humped shape in the observed light curve (see Aviles et al. 2010, Zharikov et al. 2013, and Amantayeva et al. 2021). This phenomenon is expected to happen in short-period CVs with low mass ratios ($q \lesssim 0.1$), where the enlarged Roche lobe of the primary allows the accretion disk to extend out to the 2:1 resonance radius.

The long-term light curve of GALEX J125751.4-283015 was constructed using optical photometry from the Catalina Real-time Transient Survey (CRTS; Drake et al. 2009), Asteroid Terrestrial-impact Last Alert System (ATLAS; Tonry et al. 2018), and All-Sky Automated Survey for Supernovae (ASAS-SN; Shappee et al. 2014, Kochanek et al. 2017) surveys (see Fig. A.1 lower panel). The light curve shows that GALEX J125751.4-283015 remains the majority of the time in a quiescent state (at ∼18 mag), with only two records of enhanced activity from both ATLAS and ASAS-SN, a superoutburst in August 2018 lasting around 9 months with a maximum magnitude of ∼9.8 and an outburst in May 2022 lasting around 3 months with a maximum magnitude of ∼11.4. This low number of outbursts recorded in around 20 years of data is indicative of low mass accretion rate systems such as period-bouncers. The TESS two-

minute cadence light curves as well as the SDSS spectrum are taken during periods of quiescence, and can therefore be used to derive reliable parameters of the system.

Considering that there are no available spectra of GALEX J125751.4-283015 covering the infrared wavelengths, our approach was to use the SED (constructed as detailed in Muñoz-Giraldo et al. 2024a) to obtain an approximate spectral type for the donor. Photometry from GALEX, *Gaia*, VHS, and AllWISE were used to construct the SED of GALEX J125751.4-283015 (see Fig. A.1 upper right panel). To derive the parameters of the individual components from the SED, we used the Virtual Observatory SED Analyzer (VOSA, Bayo et al. 2008). We initially fit a WD model (Koester 2010) to the SED, giving as an input a range of ±1000 K around the WD temperature of 12 000 K, the lowest value we derived from the SDSS spectrum and GALEX photometry (see Appendix B). The final WD parameters from the best fit are $T_{\rm eff}$ = 12 000 ± 125 K and $\log(g) = 8.0 \pm 0.125$, with VOSA suggesting an excess starting in the WISE1 band (consistent with findings for known period-bouncers; Muñoz-Giraldo et al. 2024a). The model binary fit tool from VOSA allows fitting of the SED simultaneously with two models, in our case a WD model (Koester 2010) and a late-type star model (BT-Settl; Allard et al. 2003). We fixed the WD parameters on the previously derived values. The best fit binary model results in a secondary component with $T_{\rm eff} = 2000 \pm 25$ K and $\log(g) = 4.5 \pm 0.25$. In the case in which the entire contribution of the secondary component can be attributed to the donor star, it would correspond to a spectral type of L0 according to the standard evolutionary track for CVs (Knigge et al. 2011). However, considering that it is very likely that part of this secondary contribution is coming from the accretion disk (Pala et al. 2018, Neustroev & Mäntynen 2023), we can characterize the spectral type of the donor as L0 or later.

To summarize, according to our multiwavelength analysis GALEX J125751.4-283015 is a confirmed CV with an orbital period of 82.17 ± 0.63 min and a donor with a spectral type of L0 or later, meaning that this high-likelihood candidate is most likely a period-bouncer. A future spectroscopic detection and characterization of the donor will allow GALEX J125751.4-283015 to become part of the sample of bona fide period-bouncers.

5. Conclusions

With this work we have conclusively proven that there are previously unknown WD-dominated CVs hiding among WD catalogs, which can be identified through the use of X-rays and which constitute a sample of high-likelihood period-bounce candidates. The application of similar search strategies has already produced the recent discovery of two new period-bouncers (WD J18204-0422 and WD J19070+2052; Cunningham et al. 2025), which were identified from a search for soft X-ray emission from likely single WDs in the *XMM-Newton* source catalog.

We explored the possible X-ray emission of *Gaia*-identified WDs and found 601 of them that appear to have a reliable eROSITA counterpart, constituting the eROSITA WD subsample. This subsample includes several single WD candidates with effective temperatures larger than 25 000 K, twice as much as the expectations for period-bouncers. Friedrich et al. (2025) used the eROSITA X-ray emission of systems in the Gentile Fusillo et al. (2021) WD catalog to identify 264 single WD candidates in the western Galactic half sky. Our parallel confirmation campaigns should help establish if the single WD candidates are indeed isolated objects or CVs. Additionally, *Gaia* astrometry of members of the eROSITA WD subsample reveals that 122 most likely are part of a resolved binary. The X-ray emission in this case could be associated with the wide companion (not the WD, meaning it is most likely a single cool WD), or could indeed be originating from an unresolved interacting binary in a triple system configuration. Shariat et al. (2025) found ∼50 CVs in such configurations, including two confirmed period-bouncers (V1108 Her and 1RXS J10142+0638), making it likely that we might find such systems in our search for period-bouncers. Future detailed studies of these potential binaries in our eROSITA WD subsample will reveal if they are a triple system with an inner CV or a wide WD binary system.

The selection cuts and a reduced version of the period-bouncer scorecard by Muñoz-Giraldo et al. (2024a) were applied to the eROSITA WD subsample to identify 161 high-likelihood period-bounce candidates. Five high-likelihood period-bounce candidates that had already been classified as CVs in the literature (CP Tuc, ASSASN -17el, ASSASN -18fk, PM J11384+0619, and Gaia 18ctg) are now confirmed as new period-bouncers, with photometrically detected donors ranging from spectral types L9.3 to T. Future detailed spectroscopic studies will help confirm the spectral type of the donors, and shed more light on their status as period-bouncers. Follow-up of Gaia DR3 2930889294867085440, a RR Lyr variable candidate, is required to proceed with its confirmation as a period-bouncer.

The ongoing effort to confirm high-likelihood period-bounce candidates that have only been identified as WDs in the literature has produced its first successful case, with the reclassification of GALEX J125751.4-283015 as a period-bouncer. This proves the capabilities of our period-bounce scorecard and selection cuts to identify period-bouncers hiding in WD catalogs, suggesting that there are several additional systems waiting to be discovered that could represent the missing population of period-bouncers.

The addition of six newly confirmed period-bouncers (five previously known CVs and one WD candidate) represents an increase in the population of some 20%, bringing the number of this elusive class of CVs to 39 systems. Within 500 pc period-bouncers now make-up 17% of eROSITA-detected CVs, comparable to the 7–25% fraction estimated for a 150 pc volume limited sample of CVs (Pala et al. 2020, Rodriguez et al. 2025). Considering that the known population of period-bounce CVs still remains well below the numbers expected by theoretical models, we foresee that further exploitation of eROSITA data will boost the population number even to the predicted levels, especially considering that the confirmation of high-likelihood period-bounce candidates around the eROSITA sensitivity limit is on its way.

The confirmation of the remaining 136 high-likelihood period-bouncers with a WD classification from SIMBAD, which is presently ongoing, is the most likely path for finding the missing population of period-bouncers. This could result in the validation of present-day evolution models for CVs without requiring a revision of the predicted numbers of systems.

Acknowledgements. Daniela Muñoz-Giraldo was supported by Deutsche Forschungsgemeinschaft (DFG) under grant number STE 1068/6-1. Santiago Hernández-Díaz acknowledges financial support from Deutsche Forschungsgemeinschaft (DFG) under grant number STE 1068/6-2. This work is based on data from eROSITA, the soft X-ray instrument aboard SRG, a joint Russian-German science mission supported by the Russian Space Agency (Roskosmos), in the interests of the Russian Academy of Sciences represented by its Space Research Institute (IKI), and the Deutsches Zentrum für Luft- und Raumfahrt (DLR). The SRG spacecraft was built by Lavochkin Association (NPOL) and its subcontractors, and is operated by NPOL with support from the Max Planck Institute for Extraterrestrial Physics (MPE). The development and construction of the eROSITA X-ray instrument was led by MPE, with contributions from the Dr. Karl Remeis Observatory Bamberg & ECAP (FAU

Erlangen-Nuernberg), the University of Hamburg Observatory, the Leibniz Institute for Astrophysics Potsdam (AIP), and the Institute for Astronomy and Astrophysics of the University of Tübingen, with the support of DLR and the Max Planck Society. The Argelander Institute for Astronomy of the University of Bonn and the Ludwig Maximilians Universität Munich also participated in the science preparation for eROSITA. The eROSITA data shown here were processed using the eSASS/NRTA software system developed by the German eROSITA consortium. This work has made use of data from the European Space Agency (ESA) mission *Gaia* (https://www.cosmos.esa.int/gaia), processed by the *Gaia* Data Processing and Analysis Consortium (DPAC, https://www.cosmos.esa.int/web/gaia/dpac/consortium). Funding for the DPAC has been provided by national institutions, in particular the institutions participating in the *Gaia* Multilateral Agreement. This publication makes use of VOSA, developed under the Spanish Virtual Observatory (https://svo.cab.inta-csic.es) project funded by MCIN/AEI/10.13039/501100011033/ through grant PID2020-112949GB-I00. VOSA has been partially updated by using funding from the European Union's Horizon 2020 Research and Innovation Programme, under Grant Agreement n° 776403 (EXOPLANETS-A). Funding for the Sloan Digital Sky Survey V has been provided by the Alfred P. Sloan Foundation, the Heising-Simons Foundation, the National Science Foundation, and the Participating Institutions. SDSS acknowledges support and resources from the Center for High-Performance Computing at the University of Utah. SDSS telescopes are located at Apache Point Observatory, funded by the Astrophysical Research Consortium and operated by New Mexico State University, and at Las Campanas Observatory, operated by the Carnegie Institution for Science. The SDSS web site is www.sdss.org. SDSS is managed by the Astrophysical Research Consortium for the Participating Institutions of the SDSS Collaboration, including the Carnegie Institution for Science, Chilean National Time Allocation Committee (CNTAC) ratified researchers, Caltech, the Gotham Participation Group, Harvard University, Heidelberg University, The Flatiron Institute, The Johns Hopkins University, L'Ecole polytechnique fédérale de Lausanne (EPFL), Leibniz-Institut für Astrophysik Potsdam (AIP), Max-Planck-Institut für Astronomie (MPIA Heidelberg), Max-Planck-Institut für Extraterrestrische Physik (MPE), Nanjing University, National Astronomical Observatories of China (NAOC), New Mexico State University, The Ohio State University, Pennsylvania State University, Smithsonian Astrophysical Observatory, Space Telescope Science Institute (STScI), the Stellar Astrophysics Participation Group, Universidad Nacional Autónoma de México, University of Arizona, University of Colorado Boulder, University of Illinois at Urbana-Champaign, University of Toronto, University of Utah, University of Virginia, Yale University, and Yunnan University.

References

Allard, F., Guillot, T., Ludwig, H.-G., et al. 2003, Symposium-International Astronomical Union (Cambridge University Press), 211, 325
Amantayeva, A., Zharikov, S., Page, K., et al. 2021, ApJ, 918, 58
Araujo-Betancor, S., Gänsicke, B., Hagen, H.-J., et al. 2005, A&A, 430, 629
Audard, M., Osten, R., Brown, A., et al. 2007, A&A, 471, L63
Aviles, A., Zharikov, S., Tovmassian, G., et al. 2010, ApJ, 711, 389
Bailer-Jones, C. A. L., Rybizki, J., Fouesneau, M., Demleitner, M., & Andrae, R. 2021, AJ, 161, 147
Barba, R. 2018, ATel, 11971, 1
Bayo, A., Rodrigo, C., Barrado Y Navascués, D., et al. 2008, A&A, 492, 277
Belloni, D., Schreiber, M. R., Pala, A. F., et al. 2020, MNRAS, 491, 5717
Beuermann, K., Euchner, F., Reinsch, K., Jordan, S., & Gänsicke, B. 2007, A&A, 463, 647
Bochkarev, N. G., Karitskaia, E. A., & Shakura, N. I. 1979, Sov. Astron., 23, 8
Bowen, I. S., & Vaughan, A. H., Jr. 1973, Appl. Opt., 12, 1430
Breedt, E., Gaensicke, B. T., Girven, J., et al. 2012, MNRAS, 423, 1437
Brunner, H., Liu, T., Lamer, G., et al. 2022, A&A, 661, A1
Carrasco, J., Catalan, S., Jordi, C., et al. 2014, A&A, 565, A11
Casagrande, L., & VandenBerg, D. A. 2014, MNRAS, 444, 392
Clementini, G., Ripepi, V., Molinaro, R., et al. 2019, A&A, 622, A60
Cunningham, T., Caiazzo, I., Sienkiewicz, G., et al. 2025, MNRAS, 540, 633
De Luca, A., Stelzer, B., Burgasser, A. J., et al. 2020, A&A, 634, L13
Deloye, C. J., Bildsten, L., & Nelemans, G. 2005, ApJ, 624, 934
Drake, A., Djorgovski, S., Mahabal, A., et al. 2009, ApJ, 696, 870
El-Badry, K., & Rix, H.-W. 2018, MNRAS, 480, 4884
Farihi, J., Burleigh, M., & Hoard, D. 2008, ApJ, 674, 421
Friedrich, S., Maitra, C., Dennerl, K., et al. 2025, Astron. Nachr., 346, e20240139
Froning, C. S., Robinson, E. L., Welsh, W. F., & Wood, J. H. 1999, ApJ, 523, 399
Galiullin, I., Rodriguez, A. C., Kulkarni, S. R., et al. 2024, MNRAS, 528, 676
Gänsicke, B., Dillon, M., Southworth, J., et al. 2009, MNRAS, 397, 2170
Gentile Fusillo, N. P., Tremblay, P.-E., Gänsicke, B. T., et al. 2019, MNRAS, 482, 4570
Gentile Fusillo, N., Tremblay, P., Cukanovaite, E., et al. 2021, MNRAS, 508, 3877
Girven, J., Gänsicke, B., Steeghs, D., & Koester, D. 2011, MNRAS, 417, 1210
Goliasch, J., & Nelson, L. 2015, ApJ, 809, 80
Green, M. J., Marsh, T. R., Carter, P. J., et al. 2020, MNRAS, 496, 1243
Gunn, J. E., Siegmund, W. A., Mannery, E. J., et al. 2006, AJ, 131, 2332
Harrison, T. E. 2015, ApJ, 816, 4
Hernández-Díaz, S., Stelzer, B., Schwope, A., & Muñoz-Giraldo, D. 2025, A&A, 703, A166
Hodgkin, S. T., Harrison, D. L., Breedt, E., et al. 2021, A&A, 652, A76
Horne, K., & Marsh, T. 1986, MNRAS, 218, 761
Howell, S. B., Nelson, L. A., & Rappaport, S. 2001, ApJ, 550, 897
Inight, K., Gänsicke, B. T., Breedt, E., et al. 2023a, MNRAS, 524, 4867
Inight, K., Gänsicke, B. T., Schwope, A., et al. 2023b, MNRAS, 525, 3597
Ishioka, R., Sekiguchi, K., & Maehara, H. 2007, PASJ, 59, 929
Jiménez-Esteban, F., Torres, S., Rebassa-Mansergas, A., et al. 2018, MNRAS, 480, 4505
Kawka, A., Vennes, S., Ferrario, L., et al. 2021, MNRAS, 507, L30
Kepler, S., Pelisoli, I., Koester, D., et al. 2015, MNRAS, 455, 3413
Kepler, S., Koester, D., Pelisoli, I., Romero, A. D., & Ourique, G. 2021, MNRAS, 507, 4646
King, A. 1988, QJRAS, 29, 1
Kirkpatrick, J. D., & McCarthy, D. W., Jr. 1994, AJ, 107, 333
Knigge, C., Baraffe, I., & Patterson, J. 2011, ApJS, 194, 28
Kochanek, C. S., Shappee, B. J., Stanek, K. Z., et al. 2017, PASP, 129, 104502
Koester, D. 2010, Mem. Soc. Astron. It., 81, 921
Kolb, U. 1993, A&A, 271, 149
Kolb, U., King, A., & Ritter, H. 1998, MNRAS, 298, L29
Kollmeier, J., Anderson, S., Blanc, G., et al. 2019, BAAS, 51, 274
Kollmeier, J. A., Rix, H.-W., Aerts, C., et al. 2025, AJ, 171, 52
Kunze, S., & Speith, R. 2005, ASP Conf. Ser., 330, 389
Le Guillou, L., Mitra, A., Baumont, S., et al. 2015, ATel, 7068, 1
Levitan, D., Groot, P. J., Prince, T. A., et al. 2015, MNRAS, 446, 391
Littlefair, S., Dhillon, V., & Martin, E. 2003, MNRAS, 340, 264
Mason, E., & Howell, S. 2005, A&A, 439, 301
McAllister, M., Littlefair, S., Dhillon, V., et al. 2017, MNRAS, 467, 1024
McAllister, M., Littlefair, S., Parsons, S., et al. 2019, MNRAS, 486, 5535
Mennickent, R., & Diaz, M. P. 2002, MNRAS, 336, 767
Merloni, A., Lamer, G., Liu, T., et al. 2024, A&A, 682, A34
Muñoz-Giraldo, D., Stelzer, B., de Martino, D., & Schwope, A. 2023, A&A, 676, A7
Muñoz-Giraldo, D., Stelzer, B., & Schwope, A. 2024a, A&A, 687, A305
Muñoz-Giraldo, D., Stelzer, B., & Schwope, A. 2024b, RNAAS, 8, 279
Nauenberg, M. 1972, ApJ, 175, 417
Nelemans, G., Zwart, S. P., Verbunt, F., & Yungelson, L. 2001, A&A, 368, 939
Neustroev, V. V., & Mäntynen, I. 2023, MNRAS, 523, 6114
Neustroev, V., Marsh, T. R., Zharikov, S., et al. 2017, MNRAS, 467, 597
Owens, D., Xu, S., Manjavacas, E., et al. 2023, AJ, 166, 5
Paczynski, B. 1976, Symposium-International Astronomical Union (Cambridge University Press), 73, 75
Paegert, M., Stassun, K. G., Collins, K. A., et al. 2022, VizieR On-line Data Catalog: IV/39
Pala, A. F., Schmidtobreick, L., Tappert, C., Gänsicke, B. T., & Mehner, A. 2018, MNRAS, 481, 2523
Pala, A. F., Gänsicke, B. T., Marsh, T., et al. 2019, MNRAS, 483, 1080
Pala, A., Gänsicke, B., Breedt, E., et al. 2020, MNRAS, 494, 3799
Pala, A., Gänsicke, B., Belloni, D., et al. 2022, MNRAS, 510, 6110
Patterson, J. 1998, PASP, 110, 1132
Patterson, J. 2011, MNRAS, 411, 2695
Patterson, J., Thorstensen, J. R., & Kemp, J. 2005, PASP, 117, 427
Predehl, P., Andritschke, R., Arefiev, V., et al. 2021, A&A, 647, A1
Pretorius, M. L., Knigge, C., & Schwope, A. D. 2013, MNRAS, 432, 570
Ramsay, G., Green, M., Marsh, T., et al. 2018, A&A, 620, A141
Ricker, G. R., Winn, J. N., Vanderspek, R., et al. 2015, J. Astron. Telesc. Instrum. Syst., 1, 014003
Rodriguez, A. C., El-Badry, K., Suleimanov, V., et al. 2025, PASP, 137, 014201
Santisteban, J. V. H., Knigge, C., Littlefair, S. P., et al. 2016, Nature, 533, 366
Santisteban, J. H., Knigge, C., Pretorius, M., Sullivan, M., & Warner, B. 2018, MNRAS, 473, 3241
Schwope, A., Kurpas, J., Baecke, P., et al. 2024, A&A, 686, A110
Shappee, B. J., Prieto, J., Grupe, D., et al. 2014, ApJ, 788, 48
Shariat, C., El-Badry, K., Naoz, S., & Rodriguez, A. C.. & van Roestel, J. 2025, PASP, accepted [arXiv:2501.14025]
Sion, E. M. 1995, ApJ, 438, 876
Sion, E. M. 1999, PASP, 111, 532
Skidmore, W., Mason, E., Howell, S. B., et al. 2000, MNRAS, 318, 429

Smak, J. 1969, Acta Astron., 19, 155
Smak, J. 1982, Acta Astron., 31, 395
Smee, S. A., Gunn, J. E., Uomoto, A., et al. 2013, AJ, 146, 32
Southworth, J., Gänsicke, B., Marsh, T., et al. 2006, MNRAS, 373, 687
Southworth, J., Hickman, R. D., Marsh, T., et al. 2009, A&A, 507, 929
Space Telescope Science Institute. 2024, MAST Portal, https://mast.stsci.edu/portal/Mashup/Clients/Mast/Portal.html Accessed: 2023-09-20
Stelzer, B., de Martino, D., Casewell, S., Wynn, G., & Roy, M. 2017, A&A, 598, L6
Sunyaev, R., Arefiev, V., Babyshkin, V., et al. 2021, A&A, 656, A132
Szkody, P., Henden, A., Agüeros, M., et al. 2006, AJ, 131, 973
Thomas, H.-C., & Reinsch, K. 1996, A&A, 315, L1
Tonry, J., Denneau, L., Heinze, A., et al. 2018, PASP, 130, 064505
Torres, S., Cruz, P., Murillo-Ojeda, R., et al. 2023, A&A, 677, A159
Tremblay, P.-E., Bergeron, P., & Gianninas, A. 2011, ApJ, 730, 128
Unda-Sanzana, E., Marsh, T., Gänsicke, B. T., et al. 2008, MNRAS, 388, 889
Vincent, O., Barstow, M., Jordan, S., et al. 2024, A&A, 682, A5
Wang, J., Li, H., Xin, L., et al. 2020, AJ, 159, 35
Warner, B. 1995, Cataclysmic Variable Stars (Cambridge University Press), 28
Wesemael, F., Greenstein, J., Liebert, J., et al. 1993, PASP, 105, 761
Wilson, R. E. 2006, ASP Conf. Ser., 349, 71
Wilson, J. C., Hearty, F. R., Skrutskie, M. F., et al. 2019, PASP, 131, 055001
Zharikov, S., Tovmassian, G., Aviles, A., et al. 2013, A&A, 549, A77

Table A.1. WD temperature obtained for new period-bouncers using VOSA compared to values found in the literature.

	VOSA [K]	Literature [K]
CP Tuc	11750	10000 ± 1500 (1)
ASSASN -17el	10500	
ASSASN -18fk	12000	11000 ± 500 (2)
PM J11384+0619	11500	
Gaia 18ctg	12250	

References. (1) Beuermann et al. (2007), (2) Wang et al. (2020).

Appendix A: Photometric detection of a late-type donor

Similar to the methodology described in Muñoz-Giraldo et al. (2024a), we used the photometry available for the newly confirmed period-bouncers in order to prove the presence of a late-type donor in the system. The VOSA fit using a WD model (Koester 2010) results in the WD effective temperatures shown in Table A.1, which all agree within 18% of the published value available for two of them. The obtained WD temperature is then used for the binary fit that characterizes the excess emission over the contribution of the WD. Considering that the excess emission can be coming fully or partially from the donor this corresponds to a L9.3-type or later donor for ASASSN -17el, and a T-type donor for the other new period-bouncers (Knigge et al. 2011).

Appendix B: WD parameters from SDSS spectra and GALEX photometry

For GALEX J125751.4-283015 we have two SDSS spectra available (see Fig. B.1) that we complement with GALEX photometry. In the following, we describe the procedure used to determine the effective temperature and surface gravity of the WD.

In isolated WDs, the Balmer absorption lines are typically used to constrain the effective temperature and surface gravity by fitting a grid of WDs atmosphere models to the observed spectra. In accreting WDs, this procedure becomes more complicated due to superimposed Balmer emission lines originating from the accretion disk as well as additional continuum contributions from the accretion disk and the donor. In CVs, the WD typically maintains an effective temperature of $T_{\rm eff} \gtrsim 10000$ K, due to compressional heating from the accreted material, thus, dominating in the blue region of the optical spectrum (see e.g. Sion 1995 and Sion 1999). Continuum emission from the disk becomes increasingly important at wavelengths $\gtrsim 5000$ Å, while the donor in low mass-transfer rate systems, such as period-bouncers, is of very low mass and starts to contribute only in the near–infrared regime, that is $\lambda \gtrsim 7000$ Å.

We used a grid of pure-hydrogen, Local Thermodynamic Equilibrium (LTE) WD atmosphere models (Koester 2010) covering $T_{\rm eff} = 8000 - 20000$ K in steps of 250 K and log(g)=6.5 - 9.5 in steps of 0.25. The WD models were interpolated to the wavelengths of the observed spectrum using a cubic spline. To match the spectral resolution of the SDSS data, the WD models were then convolved with the Gaussian instrumental profiles of the SDSS observed spectra. To further constrain $T_{\rm eff}$, we additionally use GALEX near- and far-ultraviolet photometry (obtained as detailed in Muñoz-Giraldo et al. 2024a). The ultraviolet flux is highly sensitive to $T_{\rm eff}$, making it particularly valuable for breaking degeneracies in the optical fitting. For the comparison, synthetic photometric fluxes were computed from the WD models using the GALEX near- and far-ultraviolet response functions (see Casagrande & VandenBerg 2014). To fit the WD model to an observed spectrum, we minimized a total chi-squared function which combines the spectroscopic component–evaluated over selected wavelength intervals–with the photometric components from GALEX,

$$\chi^2 = \sum_i \left(\frac{F_{{\rm obs},i}(\lambda) - K_{\rm WD} F_{{\rm model},i}(\lambda)}{\sigma_{{\rm obs},i}(\lambda)} \right)^2 \quad \text{(B.1)}$$

$$+ \sum_j \left(\frac{F_{{\rm obs,\ GALEX},j} - K_{\rm WD} F_{{\rm model,\ GALEX},j}}{\sigma_{{\rm obs,\ GALEX},j}} \right)^2, \quad \text{(B.2)}$$

where $F_{{\rm obs},i}$ and $\sigma_{{\rm obs},i}$ are the observed flux values and their uncertainties and $F_{{\rm model},i}$ are the corresponding flux values from the WD model. The terms $F_{{\rm obs,\ GALEX},j}$ and $\sigma_{{\rm obs,\ GALEX},j}$ represent the observed GALEX fluxes and their uncertainties in the far- and near-ultraviolet bands, while $F_{{\rm model,\ GALEX},j}$ are the synthetic fluxes obtained from the WD model. The scaling factor $K_{\rm WD}$ is the free parameter to optimize.

The fit of the spectroscopic component is performed over three wavelength intervals: [4010, 4060], [4150, 4290], and [4380, 4800] Å(see Fig. B.1). These intervals are selected to exclude the red optical regime where the accretion disk or the donor may contribute producing excess in the continuum flux. These wavelength intervals also mask the Balmer emission cores from the accretion disk, while capturing the broad wings of the Balmer absorption lines from the WD, helping to constrain log(g). The final best-fit model is selected from the models with low total chi-squared values (Eq. B.2), by choosing the one that shows the best agreement with the GALEX photometry.

We fit the two SDSS spectra of GALEX J125751.4-283015 using the methodology described above obtaining a log(g) between 8.0 and 8.5 and a WD effective temperature between 12000 K and 12500 K, values typical of short period CVs and known period-bouncers. Once the best fitting model was established, we can use it to estimate the WD radius and mass. Hereby, we considered that the ratio between the observed flux from the SDSS spectrum and the model surface flux represents the dilution factor, $(d/R_*)^2$, where d is the distance and R_* is the stellar radius. The two SDSS spectra of GALEX J125751.4-283015 and the distance of 180 pc reported by Bailer-Jones et al. (2021) give a WD radius between 8.01×10^8 cm and 8.93×10^8 cm. From these values, we derive the WD mass using the mass-radius relation by Nauenberg (1972), finding $0.67 M_\odot$ and $0.57 M_\odot$, from the two spectra, respectively. The mass range that we obtain for the WD is below the average value for CVs ($\approx 0.8\,M_\odot$; Pala et al. 2020, Pala et al. 2022) and would represent one of the period-bouncers with the lowest WD mass, together with V379 Vir with a WD mass of $0.64 M_\odot$ (Muñoz-Giraldo et al. 2023).

Appendix C: Keplerian rotation and variability in Hα

Because the accretion disk of CVs is centred on the WD, the Doppler shifts of the entire emission-line profiles that originate in the disk trace the orbital motion of the gas around the binary centre of mass. Figure C.1 shows the individual exposures that make up the two SDSS spectra available for GALEX J125751.4-283015–with one spectrum consisting of three exposures and the other of two–which are overplotted in the Hα region to illustrate the observed Doppler variability. As expected for a system

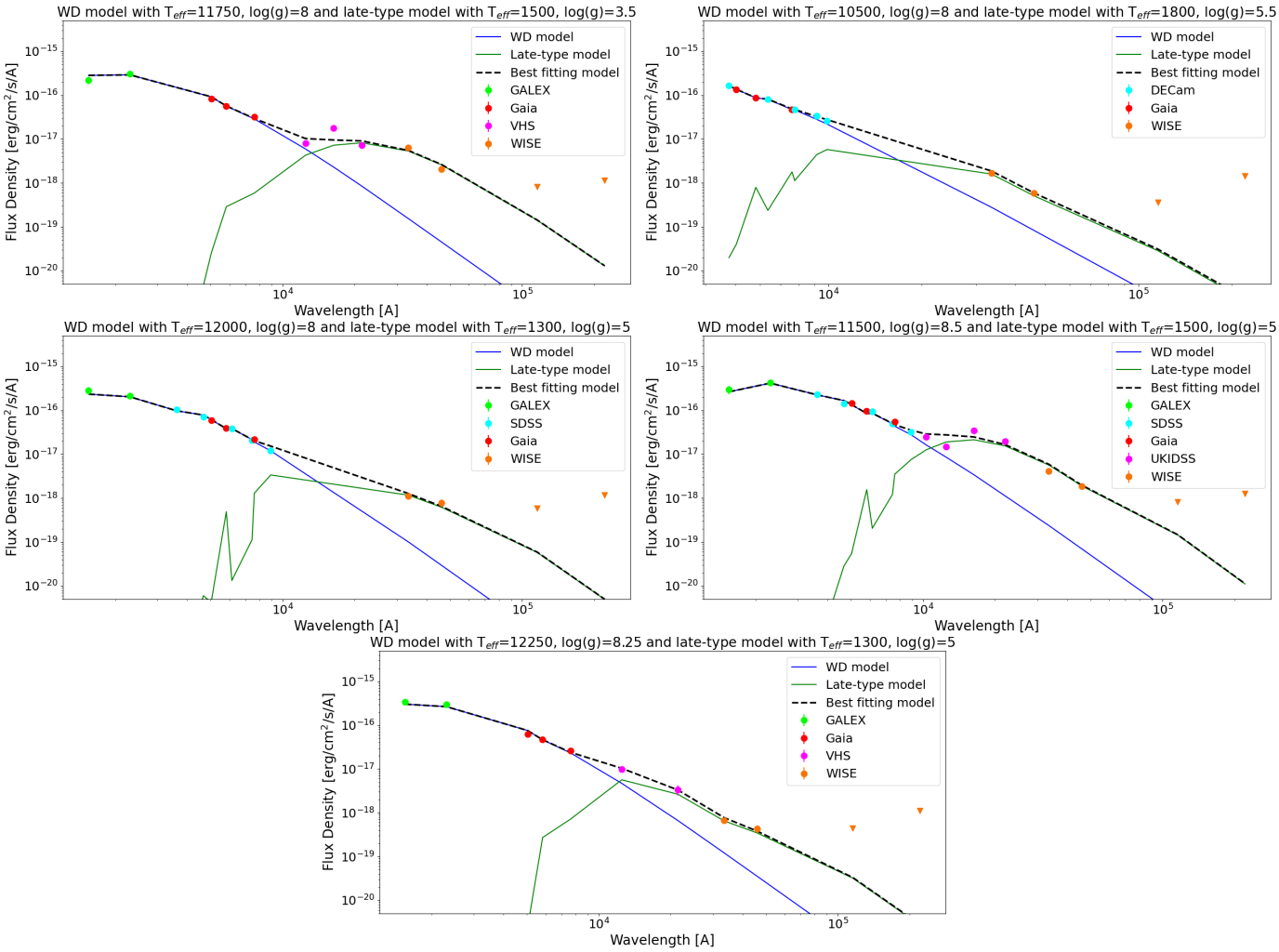

Fig. A.1. Binary fit to the SED of newly confirmed period-bouncers. Triangles show upper limits. *Upper left panel:* CP Tuc, with a temperature for the secondary component indicative of a donor with a spectral type T. *Upper right panel:* ASASSN -17el, with a temperature for the secondary component indicative of a donor with a spectral type L9.3. *Middle left panel:* ASSASN -18fk, with a temperature for the secondary component indicative of a donor with a spectral type T. *Middle right panel:* PM J11384+0619, with a temperature for the secondary component indicative of a donor with a spectral type T. *Lower panel:* Gaia 18ctg, with a temperature for the secondary component indicative of a donor with a spectral type T.

observed in quiescence (see Fig. A.1 in Sect. 4.2.2), the Hα line does not show significant variability in flux between exposures.

As can be seen in Fig. C.1, the Balmer emission lines of GALEX J125751.4-283015 show a double-peaked profile consistent with their origin in the accretion disk, with the line profile reflecting the Keplerian velocity field of the rotating gas (Smak 1969, 1982; Horne & Marsh 1986). We fit a double Gaussian to the Hα line profile in the two available SDSS spectra of the system. Since Hα predominantly traces the outer regions of the disk, the separation of the two Gaussian centroids provides an estimate of the projected Keplerian velocity, using

$$\Delta v_D = 2 v_{K,\mathrm{H}\alpha} \sin i, \tag{C.1}$$

where Δv_D is the Doppler separation between the peaks, $v_{K,\mathrm{H}\alpha}$ is the Keplerian velocity at the Hα line-forming region, and i the inclination of the accretion disk. The presence of a well-separated double-peaked profile and the absence of eclipses, as indicated by the TESS light curves (see Sect. 4.2.2), indicate a moderately inclined system. Therefore, we calculate a range of Keplerian velocities assuming inclination angles from 30° to 80°. For the two SDSS spectra, we obtained $v_{K,\mathrm{H}\alpha}$ = 568.2 − 1119.2 km/s and $v_{K,\mathrm{H}\alpha}$ = 568.5 − 1119.8 km/s respectively, values consistent with typical Keplerian velocities in the outer regions of accretion disks in CVs (see Horne & Marsh 1986).

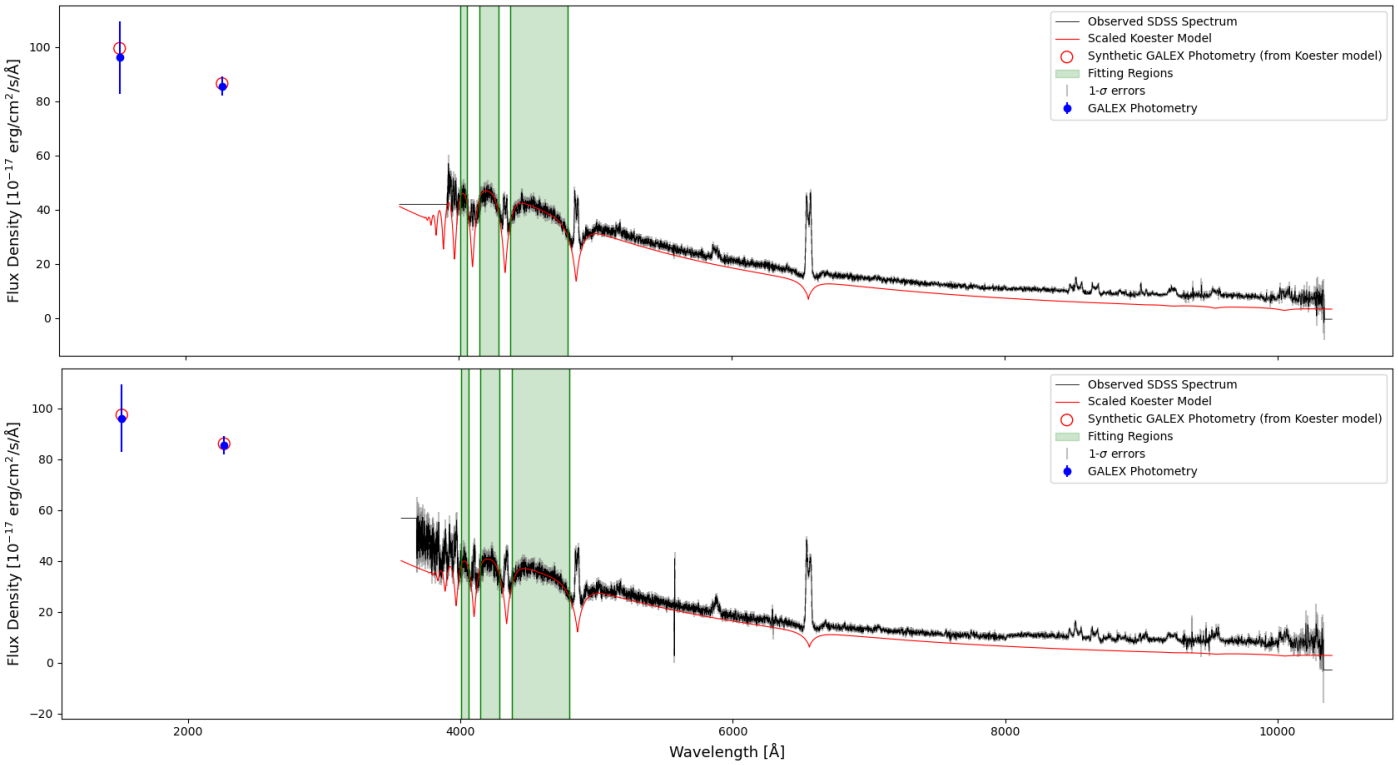

Fig. B.1. SDSS spectra and GALEX photometry of GALEX J125751.4-283015 fit with a WD model (Koester 2010). *Upper panel:* Spectrum with the best fit model characterized by log(g)=8.0 and T_{eff}=12000 K. *Lower panel:* Spectrum with the best fit model characterized by log(g)=8.5 and T_{eff}=12500 K.

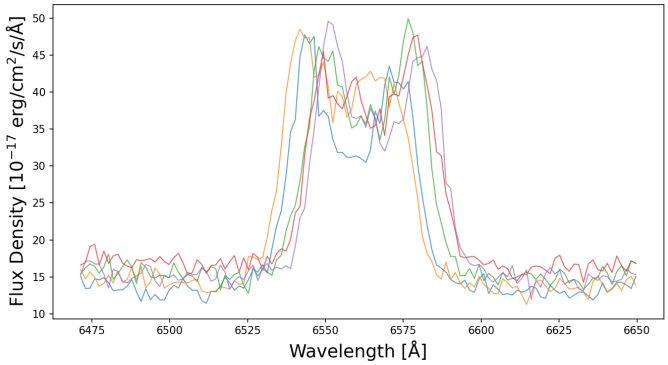

Fig. C.1. SDSS individual exposures of GALEX J125751.4-283015, overplotted to illustrate Doppler and flux variability in the Hα emission line. Each colored curve represents an individual exposure.